Avestia Publishing
Journal of Fluid Flow, Heat and Mass Transfer (JFFHMT)
Volume 3, Year 2016
ISSN: 2368-6111
DOI: 10.11159/jffhmt.2016.011

Theory and Indirect Measurements of the Drag Force Acting On a Rising Ellipsoidal Bubble

Abdullah A. Kendoush[1], Kim W. Gaines[2], Carrie W. White[2]
[1]Department of Nuclear Engineering Technology
[2]Department of Electrical & Computer Engineering Technology
akendoush@augustatech.edu, kgaines@augustatech.edu
cwcarriewild@gmail.com
Augusta Technical College
Augusta, Georgia, USA

Abstract - *A series of experiments were performed to obtain the drag force and rise characteristics of oblate ellipsoidal bubbles (OEB) in tap water at room temperature. The experiment utilized a 1.219m tall Plexiglas column with square cross section of 15.24cm sides designed and constructed for this purpose. Photographs captured the bubbles as they rose and grew vertically in the water column, and were analysed to determine the bubble radius. The drag force and velocity of rise were determined indirectly. An equation (C_D=2.667/Fr) was derived for the drag coefficient of the OEB where Fr is the Froude number. The experimental results validated this equation and earlier work by Reference [8]. The merit of this work is in the capability of the bubble's semi-major and semi-minor axes measurement being used to determine the drag coefficient and mean rising velocity of bubbles. Results were compared favourably with the current and published theoretical results.*

Keywords: Ellipsoidal bubble, Two-phase flow, Drag coefficient, Froude number.

Nomenclature

a	semi-major axis of the OEB
b	semi-minor axis of the OEB
c	semi-depth axis of the OEB
B	buoyancy force
C_D	drag coefficient
d_{eq}	equivalent diameter of the OEB
D	drag force
Eo	Eötvös number ($Eo = \Delta\rho g d_{eq}^2/\sigma$)
Fr	Froude number ($(Fr)_{OEB} = U^2/bg$ for OEB) and ($(Fr)_{SCB} = \frac{U^2}{R_{sc} f_2(\theta_m) g}$ for SCB)
g	acceleration due to gravity
M	Morton number ($M = \frac{g\mu^4\Delta\rho}{\rho^2\sigma^3}$)
OEB	oblate ellipsoidal bubble
Rc	basal radius of SCB
Re	Reynolds number ($Re=d_{eq}\rho\, U/\mu$)
R_{eq}	equivalent radius
Rsc	radius of curvature of the SCB
SCB	spherical-cap bubble
U	velocity of the OEB
We	Weber number ($We=2\rho U^2/\sigma$)
x	aspect ratio of the OEB
V	volume of the OEB
μ	absolute viscosity
ν	kinematic viscosity
ρ	density of liquid
σ	surface tension

1. Introduction

There are three main stages of bubble shape development during rise in an extended liquid: spherical, ellipsoidal, and spherical-cap (SCB). The main industrial applications of bubble dynamics are found in nuclear power generation, chemical industry, oil transportation, heating, ventilation, and air conditioning, and mineral processing.

Moore [1] analysed the motion of the OEB and obtained an equation for the variation of the drag coefficient with respect to the aspect ratio of the OEB and

Date Received: 2016-12-05
Date Accepted: 2016-10-24
Date Published: 2016-12-13

Reynolds number ($Re=Ud_{eq}/\nu$) where U is the bubble velocity, d_{eq} is the equivalent diameter, and ν is the kinematic viscosity of the liquid.

Meiron [2] solved for the distortion of the OEB from its spherical shape as the bubble velocity increased using potential flow theory. He predicted a functional relationship between Weber number($We=2\rho U^2/\sigma$) where σ is the surface tension and aspect ratio x (Fig. 1).

$$\left(x = \frac{major\ diameter\ of\ the\ cross-section\ of\ OEB}{its\ minor\ diameter} = \frac{a}{b}\right).$$

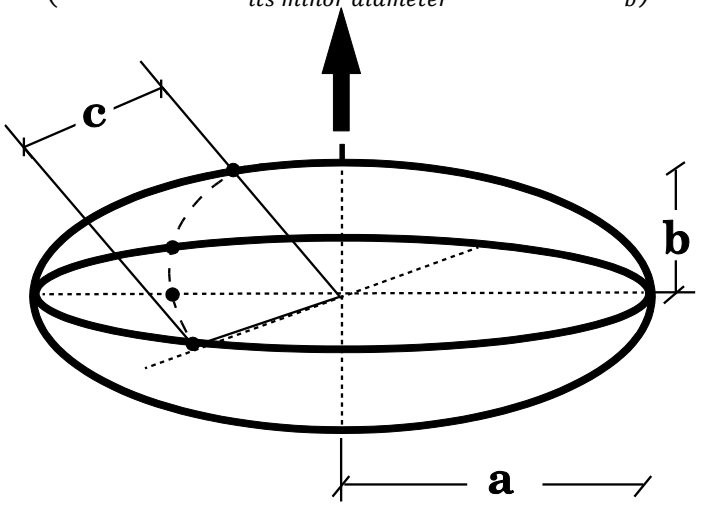

Figure 1. Geometry of the OEB (a = c).

On the experimental front, Wu and Gharib [3] concluded from their experiments that the OEB acquired a spiral path and became unstable when the bubble equivalent diameter exceeded 0.15cm or the aspect ratio exceeded 1.6. Talaia [4] performed a similar experiment to ours but used air-water system and air- glycerol system as an additional testing liquid. He acknowledged the viscosity-independence rise of a large bubble but did not make a clear distinction between the OEB and the SCB.

Wenyuan et al. [5] performed similar experiments to ours, but they used non-Newtonian aqueous solutions of polyacrylamide (PAM) and carboxymethylcellulose (CMC). Only in CMC aqueous solutions, bubbles shapes look oblate ellipsoidal similar to the ones we observed and recorded. PAM aqueous solutions produced some peculiar shaped bubbles. Aoyama et al. [6] studied the shapes of OEB's rising in infinite stagnant liquids and produced an empirical correlation for the bubble aspect ratio as a function of Eötvös and Reynolds numbers. Their definition of the aspect ratio is the reciprocal of ours. The work of Veldhuis et al.[7] revealed the existence of wakes behind the rising OEB's by using Schliern optics. They found a correspondence between these wakes and the spiraling motion of the OEB.

It appears from the literature survey that no information was provided for the experimental measurements of the drag coefficient of OEB. The main objective of this experiment was to demonstrate the possibility of measuring the dimensions of the OEB to determine its velocity and drag coefficient. In addition, some validation of previous theoretical work, by the first author, was attempted.

2. Theory

2.1. The Drag on the OEB

The drag coefficient of the OEB is defined as follows

$$C_D = \frac{D}{0.5\rho U^2 \pi (a)^2} \tag{1}$$

The drag force D in this equation was obtained by calculating the buoyancy force B acting on the OEB as these two forces oppose each other during the rise of the OEB under steady state conditions. Omitting the weight of the bubble, the buoyancy force B becomes

$$B = \frac{4}{3}\pi(a^2 b)\rho g \tag{2}$$

where ρ is the density of the liquid and g is the acceleration due to gravity. Substituting this equation in Eq. (1) and $B=D$, yields the following

$$C_D = 2.667/(Fr)_{OEB} \tag{3}$$

Here $(Fr)_{OEB} = U^2/bg$ is the Froude number that compares the inertial forces to the gravitational forces acting on the bubble. This equation shows the viscous effects and the presence of surfactants do not play a significant role on the drag particularly at high Re numbers. Ellingsen and Risso [14] arrived at similar equation but with different parameters. This specific Fr number was chosen to be based on the minor axis "b" because it is considered as the main axis responsible for the symmetry of the bubble. This specific Fr number is a more sensitive indicator of the oblateness of the bubble, than that based on the equivalent diameter normally employed by other authors.

To make the drag coefficient based on the equivalent radius, we used $C_D^* = \frac{R_{eq}}{b} C_D$.

2.2. The Drag on the SCB

The following proof is to check the validity of the drag dependence on the *Fr* number. We analyzed the case of the steady rise of the SCB. For *Re* > 100, the drag coefficient data approaches $(C_D^*)_{SCB} = 2.7$, a value obtained by many authors (e.g., [9, 10]).

The volume of the SCB (Fig. 2) is as follows [11]

$$V = \pi R_{sc}^3 f_1(\theta_m) \quad (4)$$

where θ_m is the wake angle, and $f_1(\theta_m) = \left(\frac{2}{3} - cos\theta_m + \frac{1}{3}cos^3\theta_m\right)$.

The wake angle θ_m of the SCB lies within the range of (45 – 56) degrees [12, 13]). Assuming that an average wake angle of 52 degrees was considered, Eq. (4) becomes the following

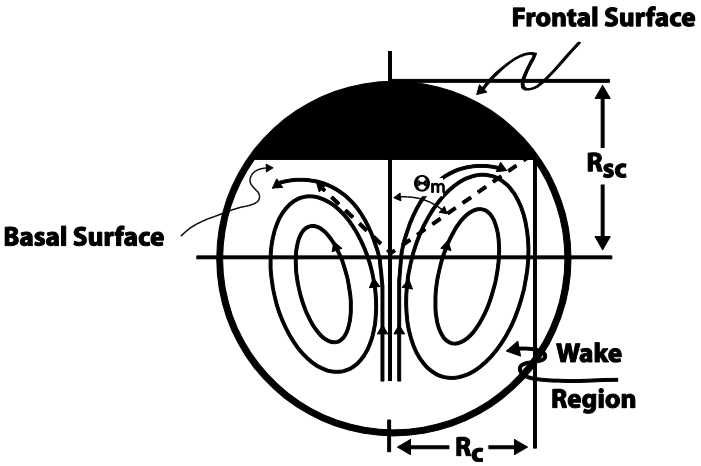

Figure 2. Idealized geometry of the spherical-cap bubble.

$$V = 0.129\pi R_{sc}^3 \quad (5)$$

It should be noted that the factor 0.129 in this equation has a range of 0.077- 0.166 based on the choice of θ_m with the average value of θ_m. The volume of an equivalent sphere corresponding to the above volume is as follows

$$V = \frac{4}{3}\pi R_{eq}^3 \quad (6)$$

Equating Eq. (4) and (5) yields,

$$R_{eq} = 0.459 R_{sc} \quad (7)$$

From the idealized geometry of the SCB (Fig. 3), we have $R_c = R_{sc} sin\theta_m$

This radius is useful in calculating the drag coefficient as it provides for the projected area as shown below

$$(C_D^*)_{SCB} = C_D\left(R_c/R_{eq}\right)^2 = 2.96 C_D \quad (8)$$

where $(C_D^*)_{SCB}$ is the drag coefficient of the SCB based on equivalent radius, and R_{eq} is the equivalent radius of the equivalent spherical volume of the SCB. Setting the drag force equal to buoyancy, the following is derived

$$C_D = \frac{\pi R_{sc}^3 f_1(\theta_m)\rho g}{0.5\rho U^2 \pi R_c^2} \quad (9)$$

Through further simplification of this equation,

$$C_D = \frac{2}{(Fr)_{SCB}} \quad (10)$$

where

$$(Fr)_{SCB} = \frac{U^2}{R_{sc} f_2(\theta_m) g} \quad (11)$$

and

$$f_2(\theta_m) = \frac{f_1(\theta_m)}{sin^2\theta_m} \quad (12)$$

Davis and Taylor [18] found in their work that

$$U = \frac{2}{3}\sqrt{R_{sc} g} \quad (13)$$

Substituting Eq. (13) into Eq. (10) yields

$$C_D = (9/2) f_2(\theta_m) \quad (14)$$

As far as the authors are aware, this new equation for the drag coefficient of the SCB was not reported before. Further, the equation needs consideration for future validation work. This is a powerful equation that

determines the drag from a single measurement of the wake angle. For $\theta_m = 52$ degrees, this equation becomes

$$C_D = 0.93 \quad (15)$$

Substituting this equation into Eq. (8), yields

$$(C_D^*)_{SCB} = 2.77 \quad (16)$$

This is the same equation of Wegener and Parlange [9] mentioned earlier. Thus, we proved that the new *Fr* number-dependent drag coefficients of Eq. (3) have some kind of validity.

3. Apparatus and Procedure

The experiments were carried out in a Plexiglas column with a 1.219m height and a cross-section of 15.2x15.2 cm (Fig. 3). The column was filled with tap water at 20 °C at atmospheric pressure.

Air was introduced into the column via an air compressor, a pressure regulated air receiver, clear vinyl tubing, and a manually operated valve. The clear tube was fitted with a glass cane-shaped appendage. The cane-shaped glass ensured the bubble would rise in the middle of the tank. A 1cc syringe with an inside needle diameter of 0.1397mm was used to introduce air bubbles into the column through a hand controlled valve. Illumination for the experiment was achieved using flood lights. A Canon camera 60D, with a Tamron SP 24-70MM F/2.8 Di VC USD lens was used with an image resolution of 0.084 x 0.081 mm/pixel (5184 x 3456 effective pixel size). The camera with a 7 fps (frames/second) rate was manually moved to ensure the bubble remained in the center of the frame of reference throughout its rise. Calibration of bubble size was accomplished via three solid spherical beads with diameters of 4.978 ±0.001mm, 3.3937±0.0001mm, and 2.972±0.001mm respectively. The beads were lowered into the rectangular column with clear fishing string. The typical distance on which the bubble was filmed was (20-30cm). No attempt was made to measure the rising speed of the camera. The camera was moved manually following the rise of the OEB bubble. The following equivalent sphere diameter was used in the processing of the data

$$d_{eq} = 2\left(\frac{3V}{4\pi}\right)^{1/3} \quad (17)$$

where V is the volume of the OEB that is given by

$$V = \frac{4}{3}\pi(abc) \quad (18)$$

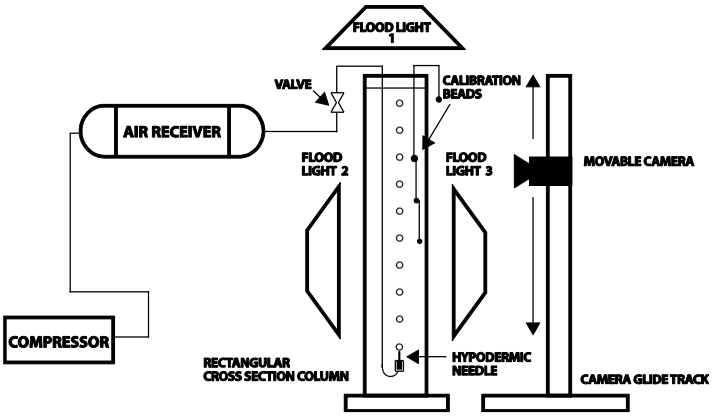

Figure 3. The experimental system.

and a is the semi-major axis, b is the semi-minor axis, and c is the semi depth axis (Fig. 1). The photographs produced a two-dimensional image with measurable a and b axes. The length c was assumed to be equal to the semi-major axis; therefore, Eq. (18) becomes

$$V = \frac{4}{3}\pi(a^2 b) \quad (19)$$

The OEB bubble velocity was not measured directly, but calculated using the following [12]

$$U = \left[\left(\frac{2.14\sigma}{\rho d_{eq}}\right) + 0.505 g d_{eq}\right]^{\frac{1}{2}} \text{(cm/s)} \quad (20)$$

d_{eq} in this equation was measured and used to calculate bubble velocity. The water properties were listed in Table 1. When the bubble detaches from the needle, its shape is spherical (x =1). As the bubble rises in the column, its shape flattens, gradually becomes OEB and its motion becomes oscillatory.

Figure 4 shows the flow regime map of the three main bubble shapes (i.e. spherical, ellipsoidal, and spherical cap) as given by Clift et al. [12]. Based on calculating *Re* number, Morton number ($M = \frac{g\mu^4\Delta\rho}{\rho^2\sigma^3}$), and Eötvös number ($Eo = \Delta\rho g d_{eq}^2/\sigma$), our experimental results fall within the OEB region (filled dots). This region was characterized by Clift et al. [9] as a wobbling

OEB. Our results were concerned with the mean rising motion and deformation of the bubble.

Our range of Re number was 506 - 979, $M = 2.569 \times 10^{-11}$, and the range of Eo was 0.415 – 2.41.

Figure 5 shows a typical photograph of the rising OEB in water with the hanging calibration beads.

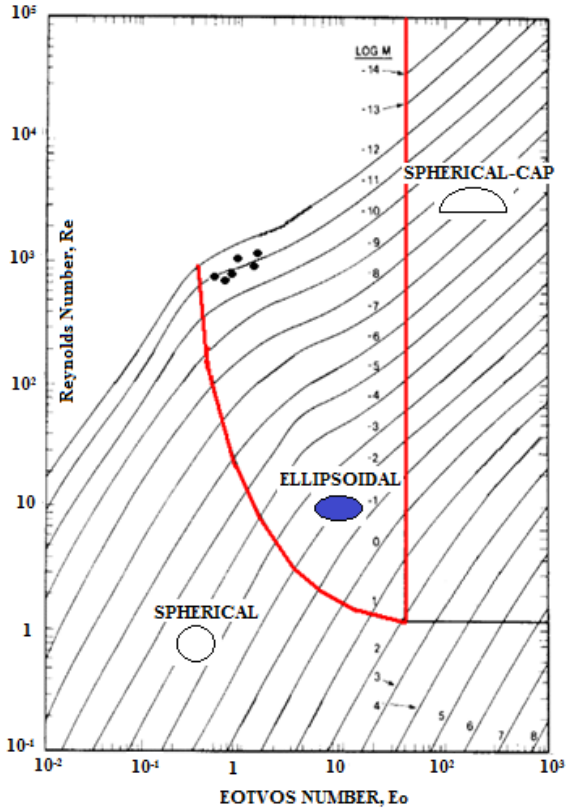

Figure 4. The flow regime map of bubbles. The filled dots are the present experimental results falling within the ellipsoidal region. The origin of this curve is Clift et al. [12].

Table 1. Water properties at 20°C.

Density kg/m^3	Surface Tension N/m	Kinematic viscosity m^2/s
998.2	72.74*10^{-3}	1.0034*10^{-6}

4. Results and Discussion

We followed the experimental evidence of Ellingsen and Risso [14] who proved the influence of surfactant of the tap water was negligible on the bubble motion. This, in addition to the derived Eq. (3), motivated us to use Eq. (20) in the present calculations of the bubble velocity, despite the fact that the equation was supposed to be applied to a clean system. The bubble emerges from the tip of the needle via a hand-regulated valve. It starts rising in spherical form, and then it changes to ellipsoidal.

Figure 6 A, B, and C show favourable comparisons between the present experimental data (particularly Fig. 6B and C) and the theoretical results of Kendoush [8], Moore [1], and Blanco and Magnuadet [15]. There is a discrepancy at x =1.5 of Fig. 6A between theory and experimental data. This can be attributed to the closeness of x =1.5 to bubble sphericity. Bubble motion in this region is rectilinear and Ellingsen and Risso [14] indicated that the rectilinear trajectory is unstable. However, Kendoush's [8] theory seems to be closer to the experimental data than both Moore [1] and Blanco and Magnuadet [15]. It should be noted that the values of the aspect ratio x was obtained directly from the photographs of the OEB, hence the photographs determined the values of x.

The newly-derived Equation (3) indicates that the drag forces are independent of viscous effects. For sufficiently high Reynolds number, the drag coefficient no longer evolves with the Re number. Figure 7 shows a close agreement between the derived Eq. (3) and the experimental data. The experimental data are based on the velocity of bubble rise obtained from Eq. (20) and the measured bubble dimension b. These velocities and b were used into $Fr = U^2/bg$ to get $C_D = 2.667/(Fr)_{OEB}$.

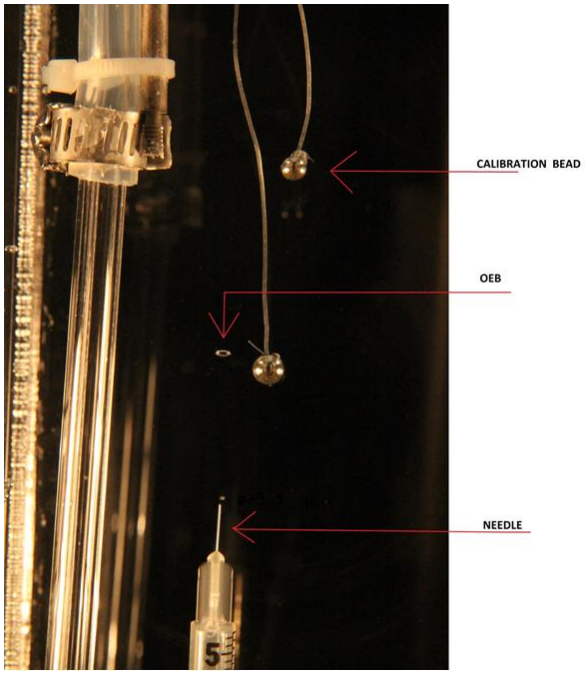

Figure 5. Typical photograph taken for the rise of the OEB in the water column.

5. Uncertainty Analysis

To find the uncertainty in the measured values of d_{eq}, we substitute Eq. (19) into (17) to get the following after simplification

$$d_{eq} = 2(a^2 b)^{1/3} \quad (21)$$

Call the uncertainty in d_{eq} as $W_{d_{eq}}$. Uncertainty can be obtained by applying the following equation (Holman [16])

$$W_{d_{eq}} = \left[\left(\frac{\partial d_{eq}}{\partial a} W_a\right)^2 + \left(\frac{\partial d_{eq}}{\partial b} W_b\right)^2\right]^{1/2} \quad (22)$$

where the uncertainty in measuring the parameter "a" is W_a = ± 0.01mm and the uncertainty in measuring b is W_b= ± 0.05 mm. Adding these errors to those reported in §3, we get $(W_a)_{total} = \sqrt{0.01^2 + 0.084^2} = \pm 0.0846$ mm and $(W_b)_{total} = \sqrt{0.05^2 + 0.081^2}$ = ± 0.0952 mm. Partial differentiating Eq. (21) and substituting in Eq. (22) yielded $W_{d_{eq}}$= ± 1.665 mm or (21.16%). Suneetha and Raghuram [17] measured the bubble diameter by using a high speed camera. They reported 18% percentage error in their measurements. The same procedure was done on Eq. (20) and yielded W_U= ± 3.596 cm/s or 9.65 %. In addition, using Eq. (3) yielded W_{C_D} = ± 0.0783 or 19.79 %.

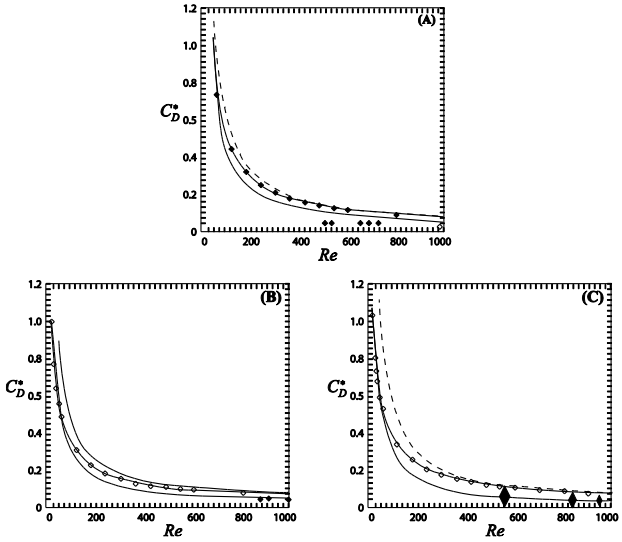

Figure 6. Comparison between the present experimental results of OEB (solid diamonds), the analytical solutions of Kendoush [8] (solid line), Moore [1] (dashed line), and the numerical solution of Blanco and Magnaudet [15] (squares on solid line). (A) x = 1.5, (B) x = 1.75, and (C) x = 1.95.

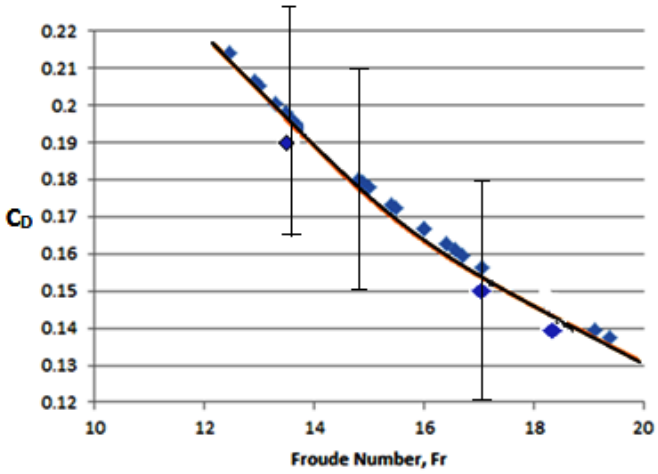

Figure 7. The present experimental data of the drag coefficient of the OEB plotted following the derived Eq. (3) (diamonds), compared with the theoretical values of Eq. (3) (Solid line).

6. Conclusion

The present work dealt with experiments on isolated air bubbles of the oblate ellipsoidal shape. Oblate ellipsoidal bubble was rising in still water. Photographs of OEB's were captured and analysed, and the data were recorded. From the photographic data, we obtained information on bubble velocity and drag. The present experimental results validated the newly-derived drag Eq. (3). This study showed that the present results also validated earlier publication of Kendoush's [8] drag equations of the OEB at high oblateness values.

Future studies will include alternate fluids, thus varied Re numbers, and aspect ratio values.

Acknowledgements

Thanks to the Southern Nuclear Company, Mr. Stephen Schroeder, Mr. J. Michael Weiksner, Sr., Dr. David M. Maryniak, and Ms. Sherrie Rowe for their efforts and support.

References

[1] D. W. Moore, "The velocity of rise of distorted gas bubbles in a liquid of small viscosity," *J. Fluid Mech.*, vol. 23, pp. 749-766, 1965.

[2] D. I. Meiron, "On the stability of gas bubbles rising in an in viscid fluid," *J. Fluid Mech.*, vol. 198, pp. 101-114, 1998.

[3] M. Wu and M. Gharib, "Experimental studies on the shape and path of small air bubbles rising in clean water," *Phys. Fluids*, vol. 14, pp. L49- L52, 2002.

[4] M. A. R. Talaia, "Terminal velocity of a bubble rise in a liquid column," *Int. J. Mathematical, Computational, and Quantum Engineering*, vol. 1, pp. 214-218, 2007.

[5] F. Wenyuan, M. Youguang, J. Shaokun, Y. Ke and L. Huaizhi, "An experimental investigation for bubble rising in non-Newtonian fluids and empirical correlation of drag coefficient," *ASME J. Fluids Engineering*, vol. 132, pp. 021305-1 - 021305-7, 2010.

[6] S. Aoyama, K. Hayashi, S. Hosokawa and A. Tomiyama, "Shapes of ellipsoidal bubbles in infinite stagnant liquids," *Int. J. Multiphase Flow*, vol. 79, pp. 23-30, 2016.

[7] C. Veldhuis, A. Biesheuvel and L. Van Wijngaarden, "Shape oscillations on bubbles rising in clean and tap water," *Phys. Fluid*, vol. 20, p. 040705, 2008.

[8] A. A. Kendoush, "Heat, mass, and momentum transfer to a rising ellipsoidal bubble," *Ind. Eng. Chem. Res.*, vol. 46, pp. 9232-9237, 2007.

[9] P. P. Weneger and J.-Y. Parlange, "Spherical-cap bubble," *An. Rev. Fluid Mech.*, vol. 5, pp. 79- 100, 1973.

[10] D. D. Joseph, "Rise velocity of a spherical-cap bubble," *J. Fluid Mech.*, vol. 488, pp. 213-223, 2003.

[11] A. A. Kendoush, "Theory of convective heat and mass transfer to spherical-cap bubbles," *AIChE Journal*, vol. 40, pp. 1440-1448, 1994.

[12] R. Clift, J. R. Grace and M. E. Weber, Bubbles, drops, and Particles, New York: Academic Press, 1978.

[13] J. R. Landel, C. Cossu and C. P. Caulfield, "Spherical-cap bubbles with a toroidal bubbly wake," *Phys. Fluids*, vol. 20, no. 12, pp. 122101-1-122101-3, 2008.

[14] K. Ellingsen and F. Risso, "On the rise of an ellipsoidal bubble in water: oscillatory paths and liquid-induced velocity," *J. Fluid Mech.*, vol. 440, pp. 235-249, 2001.

[15] A. Blanco and J. Magnuadet, "The structure of the axisymmetric high-Reynolds number flow around an ellipsoidal bubble of fixed shape," *Phys. Fluids*, vol. 7, no. 6, pp. 1265-1274, 1995.

[16] J. P. Holman, Experimental Methods for Engineers, New York: McGraw-Hill, Inc., 1989.

[17] T. B. Suneetha and P. T. Raghuram, "Bubble size measurements and error analysis in a gas-liquid ejector," *Indian J. Chemical Technology*, vol. 19, pp. 442-446, 2012.

[18] R. M. Davies and S. G. I. Taylor, "The mechanics of large bubbles rising through extended liquids in tubes," in *Proc. Roy. Soc.*, London, 1950.